International Journal of Offshore and Polar Engineering (ISSN 1053-5381)

Vol. 31, No. 1, March 2021, pp. 95–101; https://doi.org/10.17736/ijope.2021.jc806

http://www.isope.org/publications

Numerical Study on Interaction Between Focusing Waves with Fixed Cylinder

Bo Han, Weiwen Zhao* and Decheng Wan*†
Computational Marine Hydrodynamics Lab (CMHL), School of Naval Architecture, Ocean and Civil Engineering
Shanghai Jiao Tong University, Shanghai, China

Wave focusing is one of the mechanisms that results in the generation of extreme waves. The accurate numerical simulation of the interaction between the focusing wave with a fixed vertical cylinder is presented in this paper, and the simulation is conducted using the naoe-FOAM-SJTU solver, an in-house CFD solver for marine hydrodynamics. The generation of focusing wave is realized by the provided movement of the wavemaker, and the propagation of the wave is validated in advance. The wave elevations and the pressures around the cylinder are provided and compared with the experiment.

INTRODUCTION

For the design of coastal and offshore structures, safety is always a crucial issue. Generally, accidents in coastal and offshore structures can hardly be afforded. So from the view of design, the structures should be able to survive in the harshest sea conditions as demanded. Therefore, accurate prediction of hydrodynamic performance under extreme sea conditions is of great significance to safety.

The freak wave is dangerous for structure design. Longuet-Higgins (1974) pointed out that the freak wave could be regarded as the combination of a series of monochromatic waves with their crest focusing at a single point simultaneously, which we called focusing wave. The free surface of the focusing-wave case has drastic changes around the focusing point, which is impacted seriously with the viscosity, especially when it comes to problems of interaction between the focusing wave and offshore structures near the focusing point. Though the method of potential flow can quickly solve cases like this, the influence of viscosity can hardly be taken into consideration. In some experiments, the Keulegan-Carpenter number (1958) is out of the range that the influence of drag force can be neglected. Besides, the existence of the tank bottom also increases the influence of drag force to some degree. Hence, there remains the necessity to use a computational fluid dynamics (CFD) solver, which contains the calculation of viscosity through Navier–Stokes equations.

With the rapid development of parallel computing software and hardware, CFD has been more and more noticed and put into application in the field of ocean and coastal engineering in recent years. The approach to studying and simulating a freak wave is also a challenge for CFD. Higuera et al. (2013) and Hu et al. (2016) realized the irregular wave and even extreme wave generation with separated components in the OpenFOAM. DX Wang et al. (2019) realized wave generation with the piston-type wavemaker in the numerical wave tank.

In the area of offshore hydrodynamics, the interaction between wave and fixed vertical cylinder is a hotspot issue and basic work of great significance. A clear vision of the interaction wave elevation and loads of waves around the vertical cylinder is an important issue (Faltinsen et al., 2014). Bredmose et al. (2010) and Hildebrandt et al. (2013) simulated the interaction of breaking focusing wave and fixed structures. Westphalen et al. (2012) picked up and analyzed the nonlinear effect of interaction between the wave and vertical cylinder in the CFD numerical simulation. Chen et al. (2020) compared the wave runup of different directions around the cylinder in the experiment and the numerical simulation of the interaction between focusing waves and a vertical cylinder. Yan et al. (2015) compared the experimental and numerical results of the interaction between the focusing wave and the moving cylinder.

A CFD solver aiming to solve the problems of ship and marine engineering, naoe-FOAM-SJTU (Shen and Wan, 2016), was established based on the open-source platform OpenFOAM in modules, which can realize the functions of wave generation and absorption, 6 DOF motion of rigid body, arrangement of overset grid, etc. (JH Wang et al., 2019). Zhang et al. (2019) discussed the applications of naoe-FOAM-SJTU in the coupling hydrodynamic problems in ship and ocean engineering, including the interaction between waves and structures. In this paper, naoe-FOAM-SJTU is applied in the numerical simulation of the interaction between a focusing wave and a fixed cylinder, as a basic study on the monopile structure, which is among the most common types of installations in the area of coastal and offshore applications. This solver, but not the interFoam or interDyMFoam in OpenFOAM, is chosen because the focusing waves are expected to be the same as the experiment referred, and the given data are the position history curve of the wavemaker. These data can be directly used in the naoe-FOAM-SJTU to generate the focusing wave, while for interFoam or interDyMFoam, new boundary conditions or other wave generation method still must be coded. The free surface elevation and pressure data in certain locations are compared with experiment data.

NUMERICAL METHODS

Governing Equation

The simulation is conducted with the CFD solver naoe-FOAM-SJTU, which is based on the incompressible fluid assumption and takes viscosity into consideration. Thus, the governing equations should be written as follows:

$$\nabla \cdot \mathbf{U} = 0 \tag{1}$$

*ISOPE Member; †Corresponding author.

Received September 1, 2020; updated and further revised manuscript received by the editors January 23, 2021. The original version (prior to the final updated and revised manuscript) was presented at the Thirtieth International Ocean and Polar Engineering Conference (ISOPE-2020), Shanghai, China, October 11–16, 2020.

KEY WORDS: Focusing wave, numerical simulation, fixed cylinder, CFD.

$$\frac{\partial \rho \mathbf{U}}{\partial t} + \nabla \cdot \left(\rho \left(\mathbf{U} - \mathbf{U}_g\right) \mathbf{U}\right) = -\nabla p_d - \mathbf{g} \cdot \mathbf{x} \nabla \rho + \nabla \cdot \left(\mu_{\text{eff}} \nabla \mathbf{U}\right) + \left(\nabla \mathbf{U}\right) \cdot \nabla \mu_{\text{eff}} + \mathbf{f}_\sigma + \mathbf{f}_s \quad (2)$$

where $\mathbf{U}$ and $\mathbf{U}_g$ are the velocities of fluid and the grid nodes; ρ is the density of the fluid, which is mixed by the two phases of air and water; p_d is the dynamic pressure; $\mathbf{x}$ is the position vector; μ_{eff} is the effective dynamic viscosity; $\mathbf{f}_\sigma$ is the source term of surface tension, which has influence on the interface between the two phases; and $\mathbf{f}_s$ is also a source term that contributes to the sponge layer for wave absorption. In this study, laminar model is selected to avoid the decay of wave due to the turbulence model and guarantee the efficiency of the simulation.

Volume of Fluid Method

In the two phases problem, OpenFOAM captures the free surface information through the volume of fluid (VOF) method (Rusche, 2002), which is mainly dependent on the volume fraction. naoe-FOAM-SJTU follows to adopt that. After solving the velocity field by the pressure implicit splitting operator (PISO) algorithm, the volume fraction at the current time step can be solved with the transport equation:

$$\frac{\partial \alpha}{\partial t} + \nabla \cdot \mathbf{U} \alpha + \nabla \cdot \left(\mathbf{U} - \mathbf{U}_g\right) \alpha \left(1 - \alpha\right) = 0 \quad (3)$$

In this equation, α is the volume fraction, which indicates the volume ratio of the grid filled with water.

Dynamic Grid Technique

As to the movement of the wave generation boundary, the static mesh cannot satisfy the requirement of simulation, so we turn to the dynamic deformation mesh. The mesh velocity can be derived with Laplace's equation at each time step as follows:

$$\nabla \cdot \left(\gamma \nabla \mathbf{X}_g\right) = 0 \quad (4)$$

In this equation, $\gamma = 1/r^2$ is the quadratic inverse distance of cell center to the moving boundary of the wavemaker, and r is the distance between the grid center and the moving wall; $\mathbf{X}_g$ is the position vector of the grid.

The Simulation of Piston-type Wavemaker

In the cases of simulation, the movement of the piston-type wavemaker is given in the form of the piston position changes over time in the normal direction of wave generating boundary.

The wave is generated as a 2-D wave, which is a superposition of monochromatic wave with different frequency. As to the problem of focusing wave generation, the free surface elevation is

$$\eta\left(x, t\right) = \sum_{j=1}^{N} a_j \cos\left(k_j \left(x - x_t\right) - \omega_j \left(t - t_t\right)\right) \quad (5)$$

where x_t is the focusing position and t_t is the focusing time.

So the surface elevation of the wave generating boundary is

$$\eta\left(0, t\right) = \sum_{j=1}^{N} a_j \cos\left(-k_j x_t - \omega_j \left(t - t_t\right)\right) \quad (6)$$

The velocity of the moving boundary is also required in the solution, which can be estimated as follows:

$$U\left(t\right) = \frac{X\left(t_{i+1}\right) - X\left(t_i\right)}{t_{i+1} - t_i}, \quad t \in [t_i, t_{i+1}) \quad (7)$$

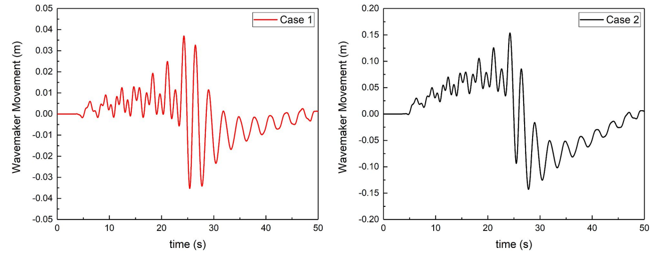

(a) Case 1 (b) Case 2

Fig. 1 History curves of wavemaker movement in x direction of experiment

CORRESPONDING EXPERIMENT SETUP

The calculation domain is designed following the experiment conducted in the Franzius-Institute Laboratory, Hannover, Germany. According to the study of Sriram et al. (2015), the tank is 110 m long, 2.2 m wide, 2 m deep, and the working depth of fresh water cases is 0.7 m in the experiment. The developed wave in a long scale of time and space appears to be different when adopting linear and second order wavemaker theory, especially when it comes to the wide range frequency spectrum, which just fits the cases of the paper. A piston-type wavemaker is on one short side of the tank. The frequency range of wave generated is 0.34 Hz~1.02 Hz (the size of the frequency range Δf = 0.68 Hz, the center frequency $f_c = 0.68$ Hz, and $\Delta f / f_c = 1$), which is separated into 32 components with same steepness in the frequency range. Focusing time is set at 38 s and the focusing location is set at 23 m from the initial position of the wavemaker. The experiment provides two cases of history curves of wavemaker movement in x direction, which is enough because the target wave to be generated is just a 2-D focusing wave. They are shown in Fig. 1. It is obvious that the amplitude of the wavemaker movement in the two cases is different; thus, the target wave heights of the two cases are also different. The maximum wave height of case 1 is about 0.1 m, while the maximum wave height of case 2 is about 0.3 m. This deviation results in the different surface elevation of focusing wave in the two cases, which is shown in the work of Sriram et al. (2021). In both cases, there are no wave-breaking phenomena in the experiment.

NUMERICAL SETUP

As to the numerical realization, there are some reasonable changes in the numerical simulation, and relative parameters are shown in Table 1. In order to generate and develop a focusing wave, there is a long distance between wave generation boundary and the preset focusing position. The cylinder is fixed even further than the focusing position. These relative positions are all kept the same as in the experiment. It is unnecessary to keep the

Parameter	Value
Length of domain	32.3 m
Width of domain	2.2 m
Height of domain	1.4 m
Depth	0.7 m
Focusing location	23 m
Cylinder location	25 m
Cylinder diameter	0.22 m
Cylinder height	1 m

Table 1 Relative parameters of the numerical domain

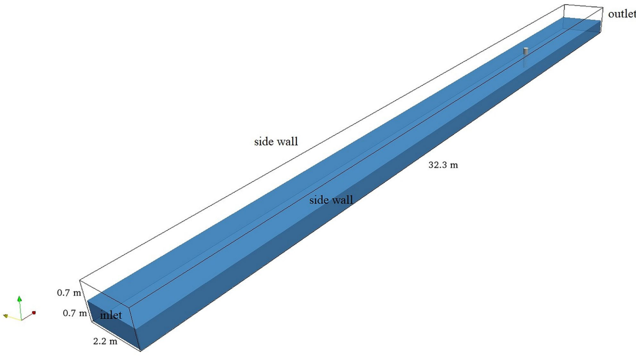

Fig. 2 Numerical domain

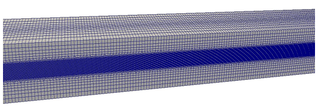

(a) Grid distribution overall

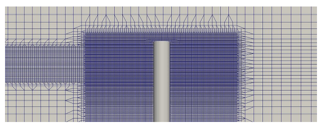

(b) Refined mesh around the cylinder

Fig. 3 Computational grid

numerical domain totally the same size as that of the experiment tank, or it will be a waste of the computational resource of time and storage. The numerical domain is designed as 32.3 m long, 2.2 m wide, 1.4 m high, and the depth of the water is set as 0.7 m.

The numerical domain is shown in Fig. 2. Figure 3 shows the computational grid distribution and the mesh around the cylinder. The mesh is generated with the blockMesh and refined with the snappyHexMesh. They are both original tools in the OpenFOAM. As the background mesh generated in the blockMesh, the numerical domain is separated into 272, 12, and 25 grids, respectively, in directions of x, y, and z. The cells around the cylinder and the free surface are refined with snappyHexMesh with the level of 2 and 3 for each. Eventually, the total number of the cells of the adopted mesh is approximately 3.18 million.

All the locations given in this study are relative to the middle of the initial location of the moving boundary of the wavemaker in directions of y and x.

Since the numerical simulation is to be compared with the experiment, in order to guarantee the correctness of the wave generation and development, not only the static setup but also the process of the wavemaker movement is necessary to ascertain as a boundary condition. The numerical simulation adopted the piston-type moving boundary, which is the same wave generation method as that of the experiment. The parameter and the piston position changes over time in the normal direction of wave generating boundary are totally the same as that of the experiment.

The setup of the wave gauges and the pressure probes is shown in Fig. 4 and Fig. 5, and the specific locations are listed in Table 2 and Table 3, respectively. It is obvious that WP1 is relatively near to the moving wall of the wavemaker, while WP4, WP5, and WP6 are around the fixed cylinder, and WP2 and WP3 are in the middle of the two groups above. The angular location of the pressure probes is the horizontal angle relative to the negative direction of the x axis. Equidistant pressure probes PP1, PP2, PP3, and PP4 are set crossing the free surface of the still water along the cylinder in z direction, and PP5 and PP6 are set on the side of the cylinder and behind the cylinder with the same vertical location of PP2.

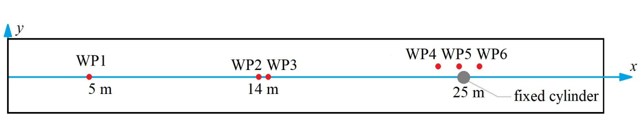

Fig. 4 Layout of the wave gauges

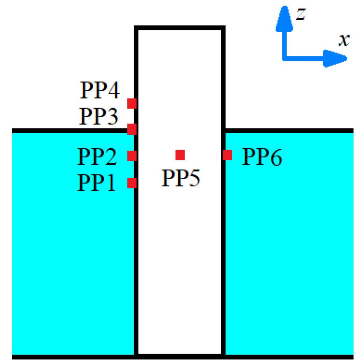

Fig. 5 Layout of the pressure probes

Wave gauges	Horizontal location / (m, m)
WP1	(4.975, 0.015)
WP2	(13.928, 0.015)
WP3	(14.428, 0.015)
WP4	(24.31, 0.275)
WP5	(24.88, 0.275)
WP6	(25.585, 0.275)

Table 2 The specific locations of wave gauges

Pressure probes	Vertical location	Angular location
PP1	0.515 m	0°
PP2	0.615 m	0°
PP3	0.715 m	0°
PP4	0.615 m	90°

Table 3 The specific locations of pressure probes

The data of the fluid field, including the volume fraction α, dynamic pressure, and velocity, are all saved in the hard disk of the PC with a certain interval set as the parameter writeInterval in the controlDict of OpenFOAM. And hindered by the storage of the PC, the interval is set as 0.2 s.

RESULTS AND DISCUSSION

First, in order to carry out the convergence analysis, three sets of mesh resolution are trialed in case 2. The amplitude of case 2 is larger in the two nonbreaking wave cases. Mesh 1, 2, and 3 are three sets of meshes for the same domain shown in the last section. The generation processes of the 3 sets are similar, and the only difference between them is the specific number of cells in the mesh. There are about 2.25 million cells in mesh 1, about 3.18 million cells in mesh 2, and about 3.89 million cells in mesh 3. Take the smallest size of the cells in z direction (which is the densest direction for cells, and most significant for the simulation of focusing wave) as an example. The smallest size of the cells in z direction of mesh 1, 2, and 3 are 0.014 m, 0.010 m, and 0.007 m, respectively.

Take the wave elevation data at WP4, for example, where the wave elevations of mesh 1, 2, and 3 are shown in Fig. 6. Compared with the result of the experiment, it is obvious that the result of mesh 2 and 3 is closer to the experiment than that of mesh 1,

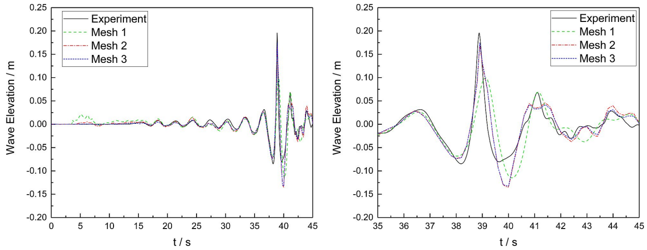

Fig. 6 Wave elevation at WP4 of different meshes

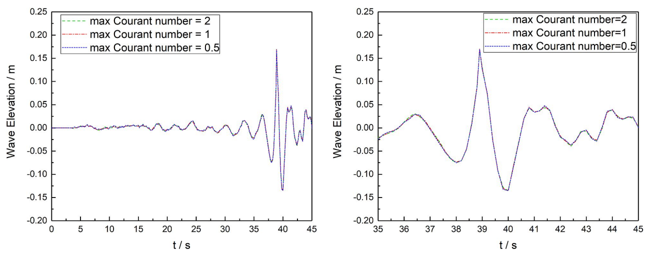

Fig. 7 Wave elevation at WP4 of different maximum Courant number

according to not only the fluctuation of the early stage, but also the largest amplitude. The difference of the result of mesh 2 and 3 is just about 3% at the largest peak, but the difference keeps and increases along with time. In order to obtain the best simulation result, mesh 3 is adopted in the following study.

Then, the convergence of the maximum of the Courant number has also been conducted. The time history curve of wave elevation with different maximum Courant numbers is shown in Fig. 7. The result is almost the same when the value of the maximum Courant number is 2, 1, or 0.5. So 1 is adopted as the maximum Courant number in the following study.

The wave elevation of case 1 is shown and compared with the experimental data in Fig. 8. As can be observed from Figs. 8a, 8b, and 8c, the generation and propagation of the focusing wave in case 1 can be guaranteed in the degree that the largest amplitude can be accurately simulated, with the deviations from the experiment less than 5%. When it comes to the wave gauges around the cylinder, namely WP4, WP5, and WP6 in Figs. 8d, 8e, and 8f, respectively, the largest amplitude is even larger, and the shape of the wave elevation history curve near the focusing location is greatly different from the symmetric shape, because of the deep trough next to the largest peak. The rough shape of the curve can also be kept in the numerical simulation, and the deviations from the experiment of the largest amplitude are about 15%.

The wave elevation of case 2 is shown and compared with the experimental data in Fig. 9. Similar to the phenomenon appearing in case 1, according to Figs. 8a, 8b, and 8c, the accuracy of generation and propagation of the focusing wave in case 2 can also be validated, and the deviations of numerical simulation from the experiment of the largest amplitude are also less than 5%. As to WP4, WP5, and WP6, which can be seen in Figs. 9d, 9e, and 9f, respectively, there is also a much larger peak, and the wave elevation history curve near the focusing location is also far from symmetry, according to the steep peaks after the largest one, which are greatly different from the case without a cylinder nearby. This phenomenon is deduced as an influence of the existence of the cylinder located 25 m from the initial location of the wavemaker. The location of the cylinder is near and after the focusing location of the wave. In the numerical simulation case, the rough shape of the curve can also be kept, and the deviations of numerical

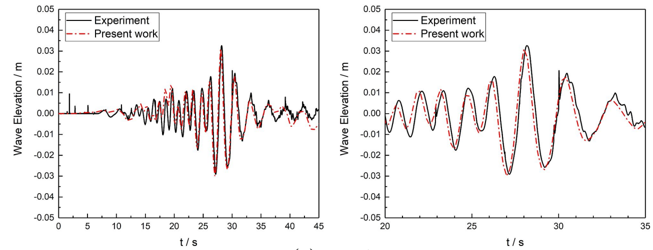

(a) WP1

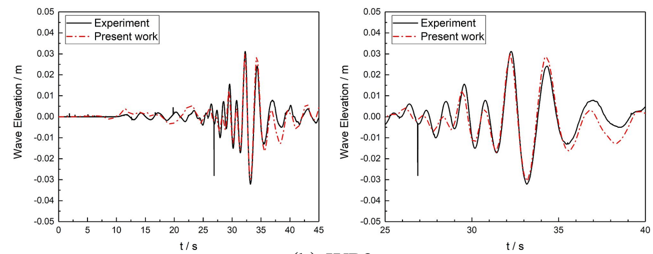

(b) WP2

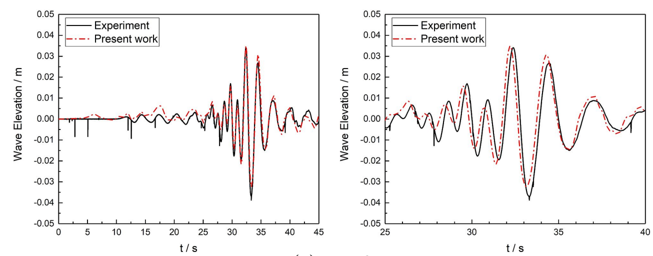

(c) WP3

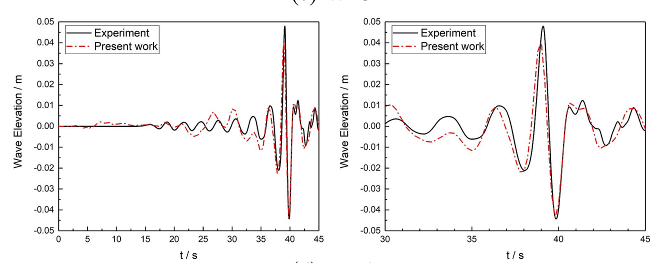

(d) WP4

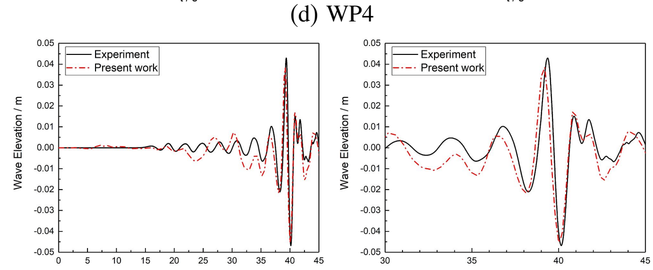

(e) WP5

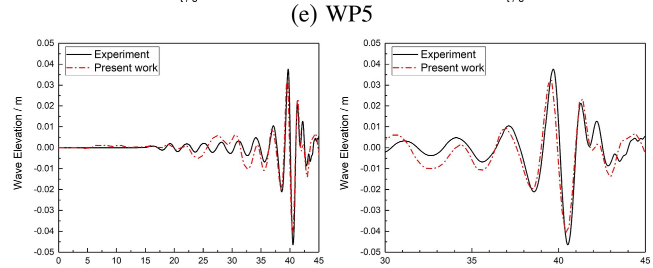

(f) WP6

Fig. 8 Wave elevation compared with the experiment of case 1

simulation from the experiment of the largest amplitude are also about 15%.

As to the differences between the numerical simulation and the experiment, especially to the deviations of the largest amplitude,

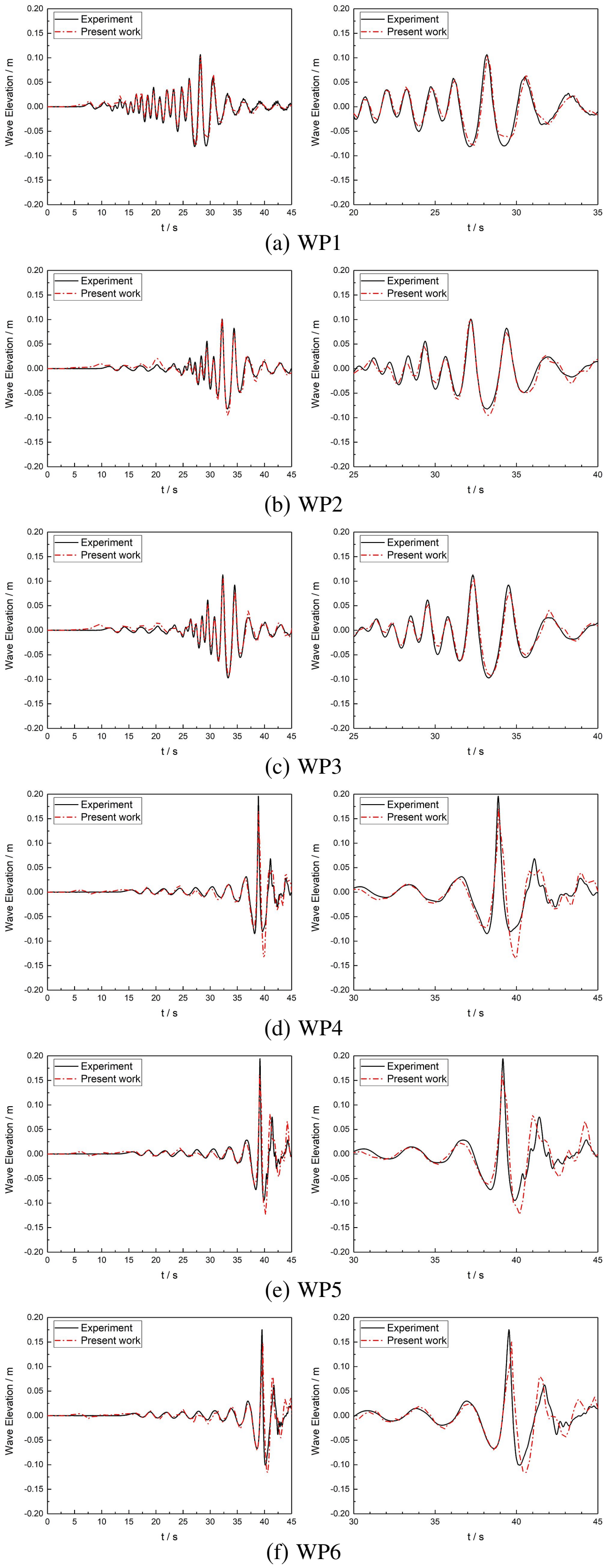

Fig. 9 Wave elevation compared with the experiment of case 2

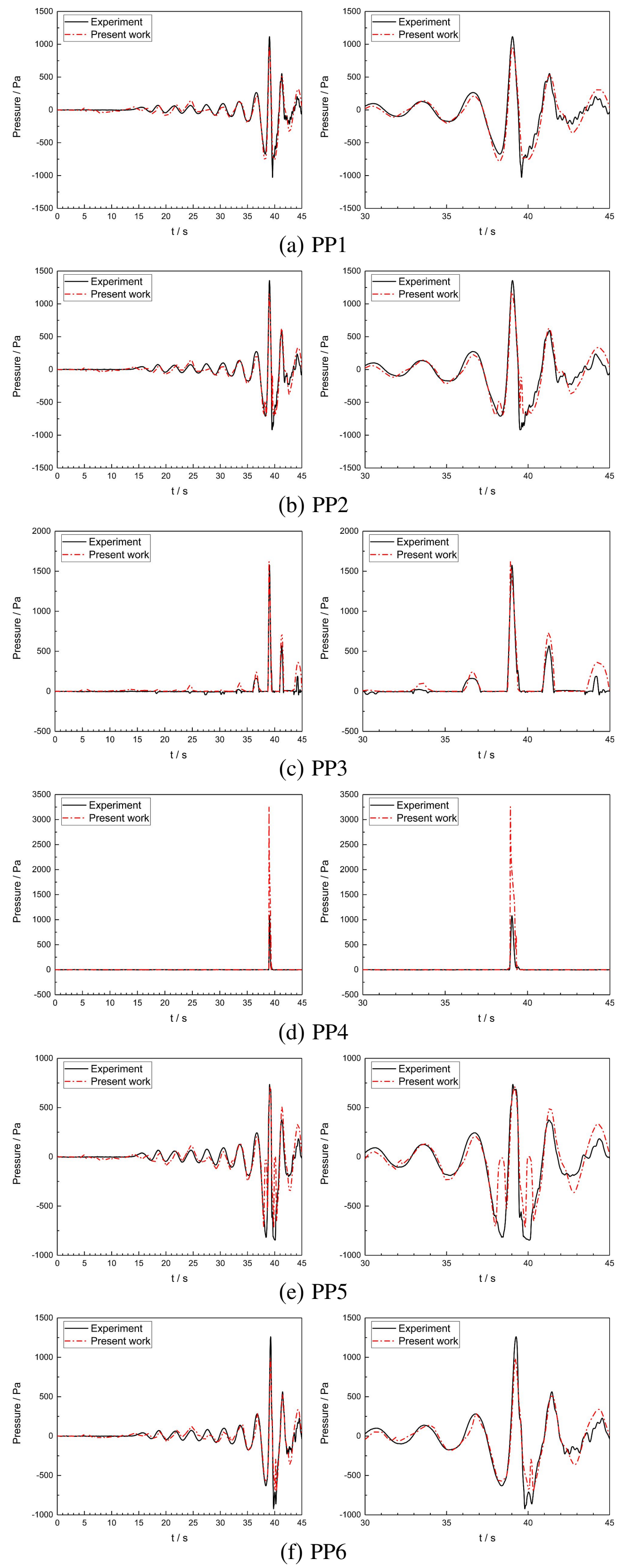

Fig. 10 Pressure compared with the experiment of case 2

the parameter writeInterval, which was introduced above, might be thought of as a key point to determine the deviations. This is because in the discrete data of the wave elevation history curve, the data around the maximum and minimum change fiercely with the even change of time. Hence, the case with denser time interval may capture the more accurate peak and trough. Otherwise, the mesh of the numerical domain, especially around the free surface and the cylinder, may also be a factor in the magnitude of deviation; the larger distance of WP4, WP5, and WP6 than that of the other three also contributes to the larger deviations. Due to the current computational condition, more complex simulations can hardly be conducted for the cases.

Take case 2, for example (its amplitude is larger than case 1), and all the phenomena are more obvious, where the pressure recorded by the probes are shown in Fig. 10. The change along with time in the numerical simulation is almost the same as in the experiment, and the differences between the numerical simulation and the experiment at their highest peak relative to the experiment of PP1 and PP3 are lower than 15%, and those of PP2 and PP5 are even lower than 4%. Meanwhile, according to Fig. 10c, as for the pressure of PP3, numerical simulation captures only positive values and 0, which is different from the experiment.

There are little peaks around the highest peak of pressure of PP2, PP5, and PP6, according to Figs. 10b, 10e, and 10f, respectively, which are just valleys in the experiment. Take the PP5 (the difference of which is the most obvious one) as an example, where the free surface around PP5 (which is colored pink) of the two little pressure peaks is shown in Fig. 11. At the two moments, PP5 is exactly at the free surface, and there is a little peak passing the side of the cylinder, which induces the peak of the little pressure peak simultaneously. As to the differences of the experiment and the numerical simulation of the present work, it is maybe traceable to the existence of the pressure probes in the experiment, which may weaken the little peak. The conjecture can also be confirmed from the side with the higher pressure of PP4 in the numerical simulation than in the experiment, according to Fig. 10d.

The free surface of case 2 around the cylinder when the focusing wave goes through is shown in Fig. 12. It can be easily observed that the cylinder hinders the continuous development of the wave. When the largest crest of the focusing wave passes through the fixed cylinder, the free surface climbs up at the shoulder of the cylinder, and ripples around the cylinder occur. When

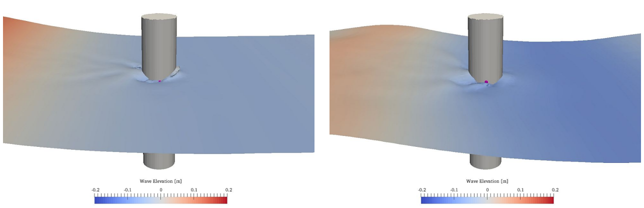

(a) $T = 39.2$ s (b) $T = 40.2$ s

Fig. 11 Free surface around the PP5

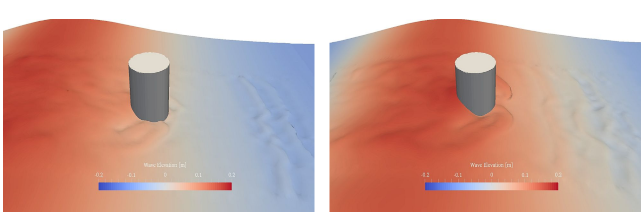

(a) $T = 39.4$ s (b) $T = 439.6$ s

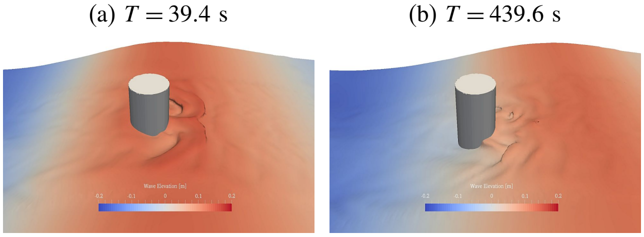

(c) $T = 39.8$ s (d) $T = 40$ s

Fig. 12 Free surface around the cylinder

the trough is drawing near to the cylinder, an obvious wave diffraction can be found on the other side of the cylinder. The phenomenon is called "ringing," which is known as a kind of nonlinear effect induced by the interaction between wave and fixed structure first in the early 1990s model test in Norway. The highly nonlinear effect of the wave–structure interaction is reproduced by Chaplin et al. (1997) and Rainey (2007) with the experiment of fixed vertical cylinder and focusing wave in a tank, where they described it. This nonlinear effect may damage the structure even more seriously than the wave itself. The little wave peaks in Fig. 11 and the wrinkles of the free surface in Fig. 12 are probably provided by the fierce interaction between the wave and the cylinder with the nonlinear dynamic characteristics of viscosity, which cannot easily be captured with potential flow method, while facilities in the experiment (such as gauges) also interfere with the occurrence of these phenomena in some degree. Thus, in order to capture these transient changes, it is significant to adopt CFD solver, which takes viscosity into consideration.

CONCLUSIONS

In the present study, the numerical simulation of the two cases of interaction between focusing wave and fixed cylinder is conducted with the CFD solver, naoe-FOAM-SJTU, which can not only qualify the generation and the propagation of the wave in a long distance, but also take the viscosity into consideration. The nonlinear dynamic characteristics of viscosity are captured as the phenomenon of the little wave peaks in the trough of focusing wave and the wrinkle of the free surface. The result of numerical simulation indicates that nonlinear influence to the wave development is derived by the existence of the fixed cylinder, which destroys the symmetry of the history curve of wave elevation around the focusing location. The difference between the simulation and the experiment of largest wave elevation amplitude is less than 5% at WP1, WP2, and WP3, but as to WP4, WP5, and WP6, which are around the cylinder, the differences are around 15%. After analysis, the reasons of the difference between the simulation and the experiment and the difference of that among the data of different wave gauges may mainly depend on the time interval of sampling, density of mesh, and the deviations induced by the existence of probes in the experiment. Besides, long distance propagation in the numerical domain may also contribute to the problem. Further optimized study still remains to be done in the future.

ACKNOWLEDGEMENTS

This work is supported by the National Natural Science Foundation of China (51879159, 51909160) and The National Key Research and Development Program of China (2019YFB1704200, 2019YFC0312400), to which the authors are most grateful.

REFERENCES

Bredmose, H, and Jacobsen, NG (2010). "Breaking Wave Impacts on Offshore Wind Turbine Foundations: Focused Wave Groups and CFD," *Proc 29th Int Conf Ocean Offshore Arct Eng*, Shanghai, China, ASME, 3, 397–404. https://doi.org/10.1115/OMAE2010-20368.

Chaplin, JR, Rainey, RCT, and Yemm, RW (1997). "Ringing of a Vertical Cylinder in Waves," *J Fluid Mech*, 350, 119–147. https://doi.org/10.1017/S002211209700699X.

Chen, QB, et al. (2020). "A Numerical Investigation of Interactions Between Extreme Waves and a Vertical Cylinder," *J Hydrodyn,* 32, 853–864. https://doi.org/10.1007/s42241-020-0055-8.

Faltinsen, OM (2014). "Hydrodynamics of Marine and Offshore Structures," *J Hydrodyn Ser B,* 26(6), 835–847. https://doi.org/10.1016/S1001-6058(14)60092-5.

Higuera, P, Lara, JL, and Losada, IJ (2013). "Realistic Wave Generation and Active Wave Absorption for Navier–Stokes Models: Application to OpenFOAM," *Coastal Eng*, 71, 102–118. https://doi.org/10.1016/j.coastaleng.2012.07.002.

Hildebrandt, A, Sriram, V, and Schlurmann, T (2013). "Simulation of Focusing Waves and Local Line Forces Due to Wave Impacts on a Tripod Structure," *Proc 23rd Int Offshore Polar Eng Conf*, Anchorage, AK, USA, ISOPE, 3, 575–581.

Hu, ZZ, Greaves, D, and Raby, A (2016). "Numerical Wave Tank Study of Extreme Waves and Wave-structure Interaction Using OpenFOAM," *Ocean Eng*, 126, 329–342. https://doi.org/10.1016/j.oceaneng.2016.09.017.

Keulegan, GH, and Carpenter, LH (1958). "Forces on Cylinders and Plates in an Oscillating Fluid," *J Res Nat Bur Stand*, 60(5), 423–440.

Longuet-Higgins, MS (1974). "Breaking Waves - in Deep or Shallow Water," *Proc 10th Symp Naval Hydrodyn*, Cambridge, MA, USA, 597–605.

Rainey, RCT (2007). "Weak or Strong Nonlinearity: The Vital Issue," *J Eng Math*, 58, 229–249. https://doi.org/10.1007/s10665-006-9126-2.

Rusche, H (2002). *Computational Fluid Dynamics of Dispersed Two-Phase Flows at High Phase Fractions*, PhD Thesis, Imperial College, London, UK.

Shen, ZR, and Wan, DC (2016). "An Irregular Wave Generating Approach Based on naoe-FOAM-SJTU Solver," *China Ocean Eng*, 30, 177–192. https://doi.org/10.1007/s13344-016-0010-1.

Sriram, V, Schlurmann, T, and Schimmels, S (2015). "Focused Wave Evolution Using Linear and Second Order Wavemaker Theory," *Appl Ocean Res*, 53, 279–296. https://doi.org/10.1016/j.apor.2015.09.007.

Sriram, V, Shagun, A, and Schlurmann, T (2021). "Laboratory Study on Steep Wave Interaction with Fixed and Moving Cylinder," *Int J Offshore Polar Eng*, ISOPE, 31(1), 19–26. https://doi.org/10.17736/ijope.2021.jc808.

Wang, DX, et al. (2019). "A Numerical Piston-type Wave-maker Toolbox for the Open-source Library OpenFOAM," *J Hydrodyn*, 31, 800–813. https://doi.org/10.1007/s42241-018-0116-4.

Wang, JH, Zhao, WW, and Wan, DC (2019). "Development of naoe-FOAM-SJTU Solver Based on OpenFOAM for Marine Hydrodynamics," *J Hydrodyn*, 31(1), 1–20. https://doi.org/10.1007/s42241-019-0020-6.

Westphalen, J, Greaves, DM, Williams, CJK, Hunt-Raby, AC, and Zang, J (2012). "Focused Waves and Wave–structure Interaction in a Numerical Wave Tank," *Ocean Eng*, 45, 9–21. https://doi.org/10.1016/j.oceaneng.2011.12.016.

Yan, S, et al. (2015). "Numerical and Experimental Studies of Moving Cylinder in Uni-directional Focusing Waves," *Proc 25th Int Ocean Polar Eng Conf*, Kona, HI, USA, ISOPE, 3, 711–718.

Zhang, XS, Wang, JH, and Wan, DC (2020). "Numerical Techniques for Coupling Hydrodynamic Problems in Ship and Ocean Engineering," *J Hydrodyn,* 32(4), 212–233. https://doi.org/10.1007/s42241-020-0021-5.